



HAL
open science

Room temperature long-range coherent exciton polariton condensate flow in lead halide perovskites

Rui Su, Jun Wang, Jiaxin Zhao, Jun Xing, Weijie Zhao, Carole Diederichs,
Timothy C.H. Liew, Qihua Xiong

► To cite this version:

Rui Su, Jun Wang, Jiaxin Zhao, Jun Xing, Weijie Zhao, et al.. Room temperature long-range coherent exciton polariton condensate flow in lead halide perovskites. *Science Advances*, 2018, 4 (10), pp.eaau0244. 10.1126/sciadv.aau0244 . hal-01935779

HAL Id: hal-01935779

<https://hal.sorbonne-universite.fr/hal-01935779>

Submitted on 27 Nov 2018

HAL is a multi-disciplinary open access archive for the deposit and dissemination of scientific research documents, whether they are published or not. The documents may come from teaching and research institutions in France or abroad, or from public or private research centers.

L'archive ouverte pluridisciplinaire **HAL**, est destinée au dépôt et à la diffusion de documents scientifiques de niveau recherche, publiés ou non, émanant des établissements d'enseignement et de recherche français ou étrangers, des laboratoires publics ou privés.



Distributed under a Creative Commons Attribution 4.0 International License

OPTICS

Room temperature long-range coherent exciton polariton condensate flow in lead halide perovskites

Rui Su¹, Jun Wang¹, Jiaxin Zhao¹, Jun Xing¹, Weijie Zhao¹, Carole Diederichs^{2,3}, Timothy C. H. Liew^{1,2*}, Qihua Xiong^{1,2,4*}

Novel technological applications significantly favor alternatives to electrons toward constructing low power-consuming, high-speed all-optical integrated optoelectronic devices. Polariton condensates, exhibiting high-speed coherent propagation and spin-based behavior, attract considerable interest for implementing the basic elements of integrated optoelectronic devices: switching, transport, and logic. However, the implementation of this coherent polariton condensate flow is typically limited to cryogenic temperatures, constrained by small exciton binding energy in most semiconductor microcavities. Here, we demonstrate the capability of long-range nonresonantly excited polariton condensate flow at room temperature in a one-dimensional all-inorganic cesium lead bromide (CsPbBr₃) perovskite microwire microcavity. The polariton condensate exhibits high-speed propagation over macroscopic distances of 60 μm while still preserving the long-range off-diagonal order. Our findings pave the way for using coherent polariton condensate flow for all-optical integrated logic circuits and polaritonic devices operating at room temperature.

INTRODUCTION

Cavity polaritons are hybrid light-matter quasi-particles arising from the quantum superposition of electron-hole pairs (excitons) and confined cavity photons. Because of the half-light and half-matter nature, these polariton eigenstates inherit from their photonic components a low effective mass and fast propagation over long distances, while the constituent excitons provide them high nonlinearity from the strong polariton-polariton interactions (1). These superior properties have led to a rich set of quantum phenomena, such as Bose-Einstein condensation (2, 3), superfluidity (4), and quantum vortices (5), as well as optoelectronic applications (6), such as polariton lasers (7, 8). One of the most notable quantum phenomena is achieving Bose-Einstein condensation at high temperatures with cavity polaritons (2, 9–12). Because of the bosonic nature of polaritons and the light effective mass, polaritons can undergo nonequilibrium Bose-Einstein condensation when their de Broglie wavelength becomes comparable to their average separation at high temperatures, involving a huge number of particles massively accumulating into one single quantum state. The single quantum state nature of a polariton condensate gives rise to the long-term temporal coherence and long-range spatial coherence, which are regarded as the basis of any quantum manipulation of the polariton condensate wave function toward all-optical coherent polariton devices.

Microcavities with various dimensionalities have demonstrated polariton condensation from cryogenic temperatures to room temperature over recent years, which include two-dimensional (2D) planar microcavities (2), 1D quantum wire microcavities (13, 14), and 0D microcavities (15, 16). In particular, 1D quantum wire microcavities hosting polaritons with high group velocity are of profound interest and importance. They hold significant promise toward the develop-

ment of optical information processing elements, including all-optical switches (17, 18), transistors (19), diodes (20), and integrated circuits (21, 22). Because of the unique symmetry of 1D quantum wire microcavities, polaritons are well confined in two of three dimensions and can only move freely in the longitudinal dimension, providing an ideal platform for all-optical manipulation (23), amplification (24), and gating of polariton condensates (17). Unlike 2D planar microcavities, the lateral discontinuity in the refractive index in 1D microcavities gives rise to the multiple subbranches of photonic modes, leading to multiple polariton branches. The multiband dispersion enables the versatility of intra- and interbranch scattering channels, which promises 1D microcavities an exceptional future for realizing phase-matching conditions in parametric amplification and optical parametric oscillation (13, 25, 26). Early research on 1D polariton microcavities started from GaAs microcavities (23, 26), which exhibit long polariton lifetime of 15 ps and long-range coherent propagation (23). Moreover, by doubling the Bragg mirror layers of a GaAs microcavity, exceptionally long polariton lifetimes on the order of 100 ps have been demonstrated, which further leads to polariton condensation in thermal equilibrium (27) and the remarkable polariton condensate propagation distance over 1 mm (28–30). However, limited by the small exciton binding energy, GaAs (23, 31) and CdTe (32) microcavities can only operate at cryogenic temperatures, which significantly hinder the development of polariton devices. Although with the robust excitons against thermal fluctuations at room temperature, wide bandgap semiconductors GaN and ZnO still experience difficulties in the patterning process to achieve low-dimensional microcavities. Recently, organic materials (9–12) with stable Frenkel excitons have been demonstrated as excellent candidates showing polariton condensation at room temperature. Although long-range propagation over hundreds of micrometers has been reported on the basis of organic Bloch surface wave polaritons (33), their condensation has not yet been achieved. In a conventional organic planar microcavity, despite the high group velocity of organic exciton polaritons, only short-range coherent polariton condensate flow limited within 10 μm has been observed due to the strong disordered environment and short polariton lifetime (34, 35). Moreover, it is not clear whether the coherence is from the pumping laser or the condensate itself, as the condensate in the organic microcavity is created under a

¹Division of Physics and Applied Physics, School of Physical and Mathematical Sciences, Nanyang Technological University, Singapore 637371, Singapore.

²MajuLab, CNRS-UNS-SU-NUS-NTU International Joint Research Unit, UMI 3654, Singapore, Singapore. ³Laboratoire Pierre Aigrain, Ecole normale supérieure, PSL University, Sorbonne Université, Université Paris Diderot, Sorbonne Paris Cité, CNRS, 24 rue Lhomond, 75005 Paris, France. ⁴NOVITAS, Nanoelectronics Center of Excellence, School of Electrical and Electronic Engineering, Nanyang Technological University, Singapore 639798, Singapore.

*Corresponding author. Email: qihua@ntu.edu.sg (Q.X.); timothy.liew@ntu.edu.sg (T.C.H.L.)

resonant pumping regime. In this context, we demonstrate, to our best knowledge, the first experimental realization of coherent polariton condensate flow at room temperature in a 1D all-inorganic CsPbBr₃ perovskite quantum wire microcavity by a nonresonant excitation. Polariton condensates with long-range coherence propagate along the quantum wire at a high group velocity of 10 μm/ps, with some polaritons propagating over 60 μm at room temperature. Moreover, we highlight that the actual polariton lifetime of 3 ps in our perovskite microcavity could be deduced through the interference fringes during the propagation process. Our technological achievements open a route to the creation of polariton-based logic elements and polariton devices working at room temperature.

RESULTS AND DISCUSSION

Unlike previous inorganic systems such as GaAs and CdTe, which significantly rely on cutting-edge epitaxial techniques, the CsPbBr₃ microwire we use here is grown by an epitaxy-free chemical vapor deposition method, which has been reported before (36–38). The whole structure of our perovskite microcavity is shown in the schematic of Fig. 1A, where the bottom mirror is 20.5 pairs of a Ta₂O₅/SiO₂ distributed Bragg reflector (DBR), while the top mirror is 8.5 pairs of a Ta₂O₅/SiO₂ DBR. Another thin layer of 65-nm SiO₂ is deposited onto the bottom DBR acting as the spacer layer before we transfer the CsPbBr₃ microwire onto the bottom DBR. Because perovskite is fragile, in the fabrication process, a thin layer of 50-nm poly(methyl methacrylate) (PMMA) is spin-coated onto the perovskite microwire to preserve the electronic and optical quality of perovskite. As shown in Fig. 1B, the effective perovskite microcavity retains the rectangular shape of the CsPbBr₃ microwire with a length of ~30 μm and a width of ~2 μm. The thickness of the perovskite microwire is ~120 nm. After the whole fabrication process, the perovskite microcavity still exhibits bright green emission under fluorescence microscopy, as shown in Fig. 1C. The realization of polariton devices at room temperature significantly demands stable excitons against thermal fluctuations. Previous studies have shown that CsPbBr₃ has stable excitons with a large exciton binding energy of 40 meV (37), as confirmed by the room temperature absorption spectrum of CsPbBr₃ in Fig. 1D. The absorption spectrum of CsPbBr₃ thin film on mica substrate (red trace) shows a strong excitonic peak centered at ~2.406 eV, while the room temperature photoluminescence (blue trace) of CsPbBr₃ exhibits a peak at ~2.353 eV with a narrow full width at half maximum

(FWHM) of 60 meV. After the CsPbBr₃ microwire is integrated into the microcavity, the emission (olive trace) from normal incidence (corresponding to in-plane wave number $k_{\parallel} = 0$) shifts to 2.297 eV, and the FWHM significantly narrows to 2.0 meV corresponding to a quality factor of ~1150 (see fig. S1 for details), suggesting that perovskite excitons are well confined in the microcavity, which is crucial toward strong coupling between excitons and cavity photons.

We then investigate the polariton behavior of the CsPbBr₃ microwire microcavity by angle-resolved photoluminescence spectroscopy at room temperature. In conventional 2D microcavities, the confinement is only along the z axis of the microcavity, which gives the wave vector quantization $k_z = \pi/L_c$, where L_c is the effective cavity length. In 1D microcavities, the additional lateral confinement along the y direction introduces an additional quantization: $k_{y,j} = (j + 1)\pi/L_y$, where L_y is the effective lateral length along the y direction and j is a new quantization number, $j = 0, 1, 2, \dots$, giving rise to multiple photonic branches that can couple to the exciton state. The relationship between the energy and wave vector of cavity modes along the x axis can be expressed as (25)

$$E_{1D}^c(j, k_x) = E_0 \sqrt{1 + \left[\frac{(j+1)\pi}{L_y} \right]^2 \frac{1}{k_z^2} + \left(\frac{k_x}{k_z} \right)^2} \quad (1)$$

where $E_0 = \hbar ck_z/n_c$. Along the y axis, the energy of each cavity mode is constant but shows electric field distribution under different k_y values. In this case, the resulting polariton dispersion exhibits multiple continuous branches along the x axis while showing multiple discrete states along the y axis. As shown in Fig. 2A, the measured polariton dispersion mapping shows continuous distribution along with the emission angle (with one-to-one mapping to the wave vector k_{\parallel}) when the long axis x of the CsPbBr₃ microwire is set to be parallel to the entrance slit of the spectrometer. Two lower polariton branches can be observed in the polariton dispersion mapping, which are caused by the strong coupling between the perovskite exciton and 1D photonic branches. The upper polariton branch can hardly be identified, which is a broadly met situation in inorganic microcavities with large Rabi splitting energy (7, 13, 36, 39, 40). However, the curvature of the measured dispersion of the lower polariton branch, which shows an S shape with a curvature tending to be smaller and smaller at large angles (see fig. S2 for details), unambiguously demonstrates the strong coupling regime. The dashed

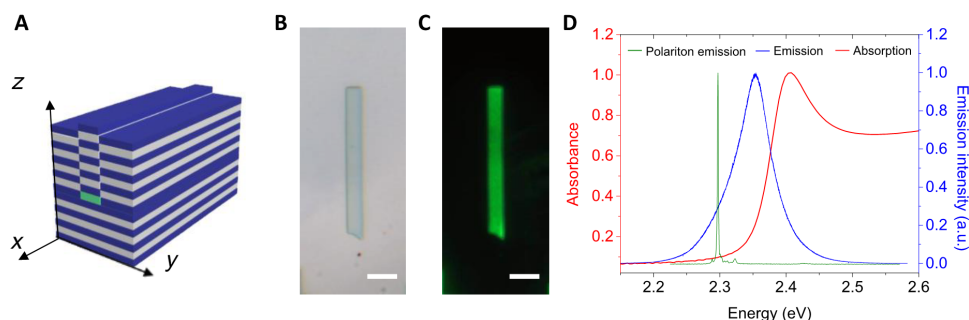


Fig. 1. Microcavity structure and characterization. (A) Schematic of the CsPbBr₃ microwire microcavity structure, showing x , y , and z axes. (B and C) Microscopy and fluorescence images of CsPbBr₃ microwire microcavity after the fabrication process under white light and blue light from a halogen lamp, respectively. Scale bars, 5 μm. (D) Room temperature photoluminescence and absorption spectra of the CsPbBr₃ perovskite. Red trace, the absorption spectrum of the CsPbBr₃ perovskite on mica substrate, showing a strong excitonic peak at ~2.406 eV. Blue trace, the photoluminescence emission spectrum of the CsPbBr₃ perovskite on mica substrate, showing an emission at ~2.353 eV with an FWHM of 60 meV. Olive trace, the ground-state emission of the CsPbBr₃ nanowire embedded into the microcavity, showing an emission at ~2.297 eV with an FWHM of ~2.0 meV. a.u., arbitrary units.

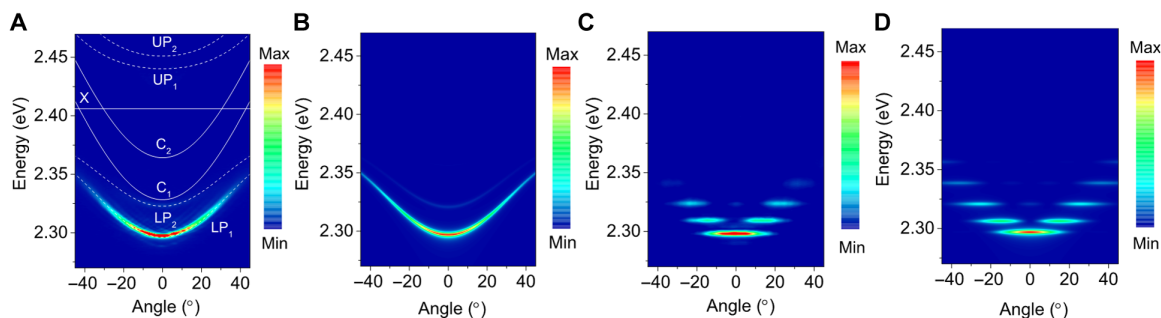


Fig. 2. Angle-resolved photoluminescence mappings of the CsPbBr₃ perovskite microwire microcavity. (A) Measured polariton emission dispersions when the long axis x is set to be parallel to the entrance slit of the spectrometer. The white dashed lines show the theoretical fitting dispersions of the upper (UP) and the lower (LP) polariton branches. The white solid lines display the dispersions of the uncoupled CsPbBr₃ perovskite exciton (X) and the cavity photon modes (C) obtained from the coupled harmonic oscillator model fitting. (B) Theoretically calculated polariton dispersions when the long axis x is set to be parallel to the entrance slit of the spectrometer. (C) Measured polariton dispersions when the short axis y is set to be parallel to the entrance slit of the spectrometer, showing multiple discrete states. (D) Theoretically calculated polariton dispersions when the short axis y is set to be parallel to the entrance slit of the spectrometer.

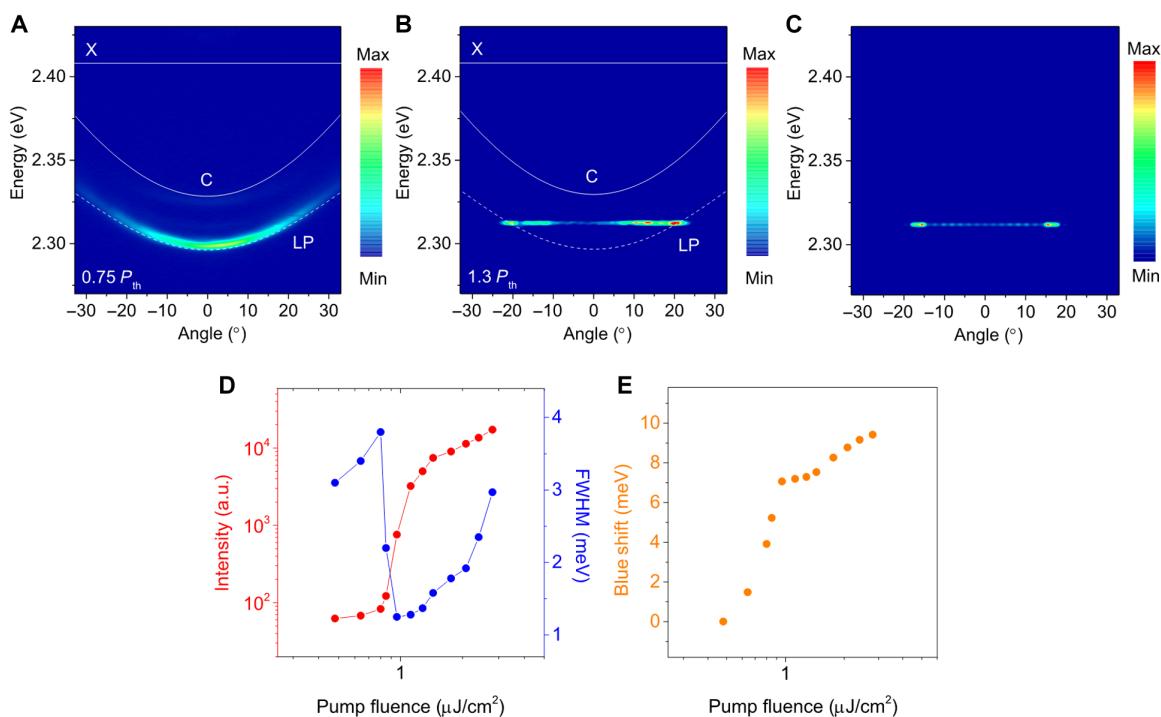


Fig. 3. Characterization of polariton condensates at room temperature. (A) Polariton dispersion at $0.75 P_{th}$, showing a broad distribution at all angles. (B) Polariton dispersion at $1.3 P_{th}$, showing symmetric dominant emission at around $\pm 20^\circ$. The polariton condensation with nonzero $k_{||}$ inclines the role of polariton propagation. (C) Simulated polariton dispersion mapping at $1.3 P_{th}$. (D) Evolution of emission intensity and linewidth as a function of pumping fluence. (E) Energy blue shift with respect to the polariton emission energy at the lowest pump fluence as a function of pump fluence.

curves in Fig. 2A show the theoretical polariton dispersions calculated by the coupled oscillator model, while the solid white lines correspond to the uncoupled exciton energy (X) and calculated cavity modes (C), respectively. From the fitting of the data, we extract the Rabi splitting energy of $2\Omega = 120$ meV with negative detunings of -80 and -40 meV. The dispersions are also theoretically well matched by assuming particle-in-a-box-type wave functions and energies for photons confined by the width of the microwire being coupled to excitons with negligible dispersion as shown in Fig. 2B. Figure 2C shows the measured polariton dispersions when the short axis y of the CsPbBr₃ microwire is set to be parallel to the entrance slit of the spectrometer, showing some discrete polariton states that are due to the electric field distribution of

cavity mode induced by the optical confinement from the small width of the CsPbBr₃ microwire, as discussed before. Similarly, the polariton discrete states can be well reproduced in theory, as shown in Fig. 2D.

The perovskite microwire microcavity is further pumped by a pulsed Ti:sapphire laser at 400 nm and a repetition rate of 1 kHz to reach non-linear regime. As shown in Fig. 3A, the lower polariton branches are observed with a broad distribution over a wide range of angles at a low pump power density of $0.75 P_{th}$ ($P_{th} = 0.8 \mu\text{J}/\text{cm}^2$). A clear blue-shift trend of polariton energy is observed, which is due to the enhanced polariton-reservoir interaction with the increase of the polariton density below the threshold, as compared with the theoretically calculated lower polariton dispersion (the white dashed line in Fig. 3A) under a low

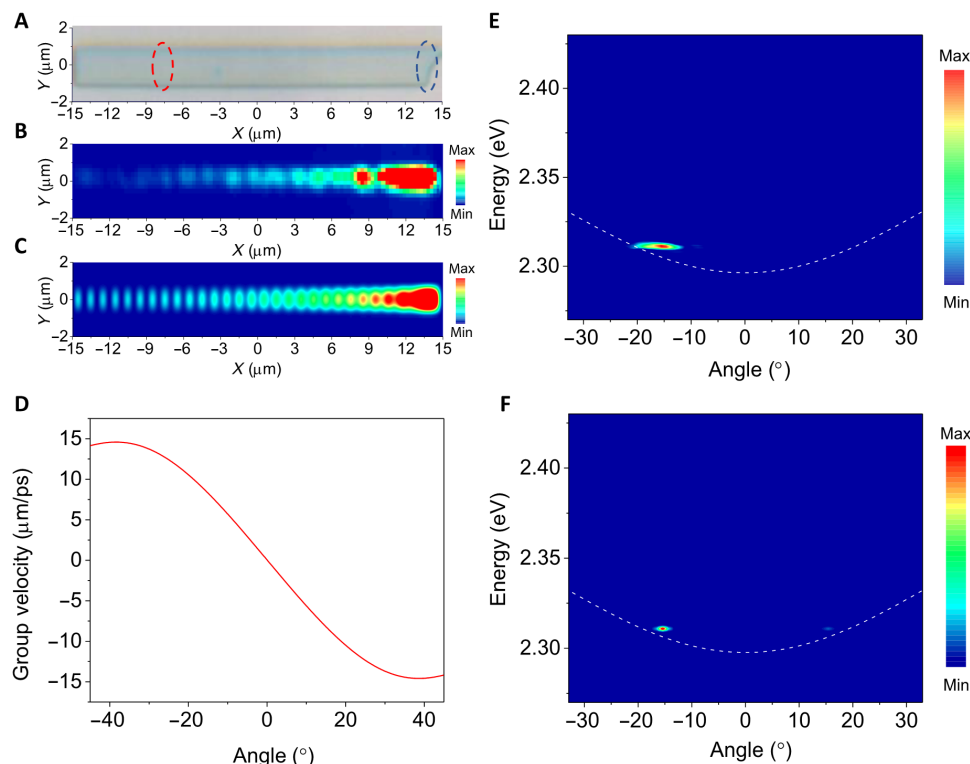


Fig. 4. Polariton condensate propagation and characterization at room temperature. (A) Schematic of pumping spot and collection spot on the microwire microcavity. (B and C) Measured and simulated real-space images of the microwire microcavity above the polariton condensation threshold, respectively. (D) Polariton group velocity extracted from the polariton dispersion as a function of emission angle (directly related to wave vector k_{\parallel}). (E and F) Measured and simulated polariton emission mappings as a function of emission angles, respectively, showing dominant emission at $\sim -15^{\circ}$.

pump power density. With the increase of the pump power density to $1.3 P_{\text{th}}$, the polariton dispersion is dominated by much stronger symmetric emissions at around $\pm 20^{\circ}$ of emission angle, which suggests the occurrence of polariton condensates. These polariton condensates at nonzero k_{\parallel} have been reported in GaAs microcavities (23, 41). The pumping of the system creates a local exciton reservoir, which feeds the condensate and also provides a localized potential peak for polaritons in real space due to polariton-exciton repulsive interactions. Polariton condensation initially occurs at the top of this potential peak, and the potential energy is converted to kinetic energy such that the polariton condensate acquires a nonzero in-plane wave vector. Thus, polariton condensates can ballistically propagate outward, leading to a large density drop below the critical density for polariton condensation. As the propagating polariton condensate is not in the ground state of the system, it can be considered as a nonequilibrium coherent condensate or quasi-condensate, which still carries the coherence from the condensation spot (28, 29). This polariton condensate behavior can be well reproduced in theory, as shown in Fig. 3C. Furthermore, when the pump power is above the condensation threshold, the real-space emission of the perovskite wire microcavity exhibits clear interference fringes (see fig. S3 for details), which implies the polariton condensate propagation behavior and the long-range spatial coherence of the polariton condensate. Further analysis of polariton propagation will be discussed later. To investigate the occurrence of polariton condensate quantitatively, we plot the polariton emission intensity and linewidth as a function of pump fluence in a log-log scale in Fig. 3D. A sharp increase of emission intensity and a rapid decrease of emission linewidth are observed when the pump fluence crosses the threshold of $P_{\text{th}} = 0.8 \mu\text{J}/\text{cm}^2$. Another im-

portant feature to demonstrate the formation of polariton condensate is the continuous blue shift with the increase of pump fluence, as shown in Fig. 3E. Two different blue-shift slopes are observed corresponding to polariton-reservoir interaction and polariton-polariton interaction, as already reported in a previous CsPbCl₃ microcavity (36). We observe a maximum blue shift of 11 meV, which is far smaller than the energy difference between the cavity mode and the polariton dispersion (30 meV). To unambiguously demonstrate the appearance of polariton condensate, we further check the spatial coherence of the emission above the threshold by interferometry measurements (see fig. S4 for details). The real-space emission of the polariton condensate is sent to a Michelson interferometer with a retroreflector configuration (2). The first-order spatial coherence $g^{(1)}(\mathbf{r}, -\mathbf{r})$ can be probed by the interference fringes' contrast between points localized at \mathbf{r} and $-\mathbf{r}$. As shown in fig. S4, clear interference fringes can be readily identified with a distance of $25 \mu\text{m}$, which suggests the buildup of long-range off-diagonal order.

Further investigations on the propagation of the polariton condensate are conducted by pumping a small area ($3 \mu\text{m}^2$) at the end of the microwire microcavity (red dashed circle), as shown in Fig. 4A. The polariton condensates are only created in the pumping spot area, and the blue-shift potential expels the condensate to propagate to the other end of the nanowire. As shown in Fig. 4B, a clear interference pattern can be observed throughout the whole microwire. To observe these interference fringes near the pumping area, polaritons have to propagate to the other end first and get reflected by the other end of the wire. They then further propagate back to the pumping area to interfere with the incoming polaritons, which proves that some polaritons have propagated

over 60 μm (twice of the wire length). To model the spatial dynamics of polariton condensates above threshold, we directly solve the driven-dissipative mean field dynamics (see Supplementary Text for details), considering the case of pulsed excitation near the microwire end. The observation of interference fringes depends on the chosen polariton decay rate in the calculation (see fig. S5 for details). As shown in Fig. 4D, the group velocity of polaritons can be obtained from the polariton dispersion according to

$$V_g = \frac{1}{\hbar} \frac{\partial E}{\partial k_{\parallel}} \quad (2)$$

We can deduce that the polariton group velocity is under 10 $\mu\text{m}/\text{ps}$. Consequently, to traverse the length of the wire (30 μm) and return to cause interference after being reflected, a polariton needs to survive for a period on the order of 5 ps or more (depending on where along the microwire we are looking for interference fringes). This corresponds to a decay rate of around 0.15 meV. In practice, not all polaritons need to survive to observe clear interference fringes, so the experiment can be supported considering slightly higher decay rates, as shown in Fig. 4C. Estimating that the polariton decay rate is around 0.2 meV upon comparison with experiment, we obtain an actual polariton lifetime of 3 ps, which is much larger than that of other microcavities working at room temperature (35). Detailed comparison between perovskite polariton condensates and other semiconductor polariton condensates has been shown in table S1. We note that this method of extracting the lifetime of polaritons is more accurate than using the linewidth, which is significantly broadened by disorder in our system. To further confirm that the obtained interference pattern results from the propagation of coherent polariton condensate, we carry out the Michelson interferometry with a retroreflector configuration. As shown in fig. S6, when the real-space image of polariton condensates above the threshold and its inverted image are superposed, clear interference fringes can be identified at the end of the wire, which confirms that spatial coherence is still preserved during the propagation process from the end to the other end of the wire. We further check the polariton dispersion in the reciprocal space to confirm the propagation of polariton condensate, as shown in Fig. 4E. The far-field emission spectrum measured at 20 μm (red circle in Fig. 4A) away from the pumping spot exhibits nonsymmetric behavior with the main emission angle at -15° , which can be explained by the dominant polariton propagation direction to the other end of the wire. With a well-defined incident in-plane wave vector, condensed polaritons can thus propagate outside the pumping area along the wire. The far-field emission spectrum matches well with the theory, as shown in Fig. 4F. The broadening of the measured polariton dispersion could be attributed to disorder in our perovskite microcavity. Similarly, the in-plane wave vector of the propagating polaritons can be well controlled by changing the pumping spot position to the other end (opposite to the blue circle in Fig. 4A). In this case, as shown in fig. S7, the far field emission shows an opposite behavior in wave vector, as compared with that shown in Fig. 4E.

CONCLUSION

In conclusion, by nonresonant optical pumping, we create a green polariton condensate with long-range coherence in an epitaxy-free CsPbBr₃ perovskite microwire microcavity at room temperature. Polaritons propagate at a high group velocity of 10 $\mu\text{m}/\text{ps}$, which is several times larger

than that of a corresponding GaAs microcavity. Meanwhile, the polariton condensate preserves the spontaneous spatial coherence during the propagation of a detectable fraction of polaritons over a macroscopic distance of 60 μm . The propagation of the polariton condensate can be readily controlled by changing the position of the pumping spot. With the long polariton lifetime and long propagation distance, perovskite 1D microcavities hold significant promise for the realization of room temperature all-optical integrated logic circuits and polaritonic devices. Last, we note that in the presence of energy traps (3), polariton relaxation often appears further enhanced. This is an important ingredient of condensate transistors (17), which could be a promising direction for future work with perovskites operated at room temperature.

MATERIALS AND METHODS

Fabrication

The bottom DBR was first fabricated by an e-beam evaporator, consisting of 20.5 pairs of silicon dioxide (87.5 nm) and tantalum pentoxide (60.2 nm). A thin layer of 65-nm SiO₂ was deposited onto the bottom DBR acting as the spacer. The CsPbBr₃ microwire was then transferred to the bottom DBR, followed by spin-coating a thin layer of 55-nm PMMA to protect the perovskite. The detailed procedure of the perovskite growth is described in our previous report (37). The substrate was then put into the e-beam evaporator again to complete the fabrication of the top DBR, which consists of 8.5 pairs of silicon dioxide (87.5 nm) and tantalum pentoxide (60.2 nm).

Optical spectroscopy characterization

Angle-resolved photoluminescence spectroscopy was measured in a homebuilt microphotoluminescence setup in the Fourier imaging configuration. The continuous-wave pump laser of 442 nm was focused on the sample surface through a high-numerical aperture (NA, 0.9) 100 \times microscope objective, covering an angular range of $\pm 64.1^\circ$. The emission from the microcavity was collected through the same objective and sent to a 550-mm focal length spectrometer (HORIBA iHR550) with a grating of 600 lines/mm and a liquid nitrogen-cooled charge-coupled device of 256 \times 1024 pixels. To reach polariton condensation, the perovskite microcavity was pumped by off-resonant excitation centered at 400 nm with a pulse duration of 100 fs and repetition rates of 1 kHz (double frequency from 800-nm laser from a Spitfire Ace Ti: sapphire regenerative amplifier by a beta barium borate crystal). The excitation laser was focused down to a $\sim 20\text{-}\mu\text{m}$ -diameter spot on the sample. The fluorescence image from the perovskite microcavity was obtained through an Olympus microscope, where the microcavity was illuminated with a halogen lamp after passing through a band-pass filter.

SUPPLEMENTARY MATERIALS

Supplementary material for this article is available at <http://advances.sciencemag.org/cgi/content/full/4/10/eaau0244/DC1>

Supplementary Text

Fig. S1. Measurement of the FWHM of polariton emission at normal incidence.

Fig. S2. Evidence of perovskite microcavity operating in strong coupling regime.

Fig. S3. Real-space images of the perovskite microcavity above the threshold.

Fig. S4. Long-range spatial coherence of the perovskite polariton condensate.

Fig. S5. Theoretically calculated time-integrated intensity pattern of polaritons generated by pulsed excitation at one end of the microwire.

Fig. S6. Long-range spatial coherence of propagating polariton condensate.

Fig. S7. Optical control of polariton condensate.

Table S1. Detailed comparison between the perovskite polariton and other semiconductor polaritons.

REFERENCES AND NOTES

- H. Deng, H. Haug, Y. Yamamoto, Exciton-polariton Bose-Einstein condensation. *Rev. Mod. Phys.* **82**, 1489 (2010).
- J. Kasprzak, M. Richard, S. Kundermann, A. Baas, P. Jeambrun, J. M. Keeling, F. M. Marchetti, M. H. Szymańska, R. André, J. L. Staehli, V. Savona, P. B. Littlewood, Bose-Einstein condensation of exciton polaritons. *Nature* **443**, 409 (2006).
- R. Balili, V. Hartwell, D. Snoke, L. Pfeiffer, K. West, Bose-Einstein condensation of microcavity polaritons in a trap. *Science* **316**, 1007–1010 (2007).
- A. Amo, J. Lefrère, S. Pigeon, C. Adrados, C. Ciuti, I. Carusotto, R. Houdré, E. Giacobino, A. Bramati, Superfluidity of polaritons in semiconductor microcavities. *Nat. Phys.* **5**, 805–810 (2009).
- K. G. Lagoudakis, M. Wouters, M. Richard, A. Baas, I. Carusotto, R. André, L. S. Dang, B. Deveaud-Plédran, Quantized vortices in an exciton-polariton condensate. *Nat. Phys.* **4**, 706–710 (2008).
- D. Sanvitto, S. Kéna-Cohen, The road towards polaritonic devices. *Nat. Mater.* **15**, 1061–1073 (2016).
- S. Christopoulos, G. B. H. von Högersthal, A. J. D. Grundy, P. G. Lagoudakis, A. V. Kavokin, J. J. Baumberg, G. Christmann, R. Butté, E. Feltn, J. F. Carlin, N. Grandjean, Room-temperature polariton lasing in semiconductor microcavities. *Phys. Rev. Lett.* **98**, 126405 (2007).
- C. Schneider, A. Rahimi-Iman, N. Y. Kim, J. Fischer, I. G. Savenko, M. Amthor, M. Lerner, A. Wolf, L. Worschech, V. D. Kulakovskii, I. A. Shelykh, M. Kamp, S. Reitzenstein, A. Forchel, Y. Yamamoto, S. Höfling, An electrically pumped polariton laser. *Nature* **497**, 348–352 (2013).
- S. Kéna-Cohen, S. R. Forrest, Room-temperature polariton lasing in an organic single-crystal microcavity. *Nat. Photonics* **4**, 371–375 (2010).
- J. D. Plumhof, T. Stöferle, L. Mai, U. Scherf, R. F. Mahrt, Room-temperature Bose-Einstein condensation of cavity exciton-polaritons in a polymer. *Nat. Mater.* **13**, 247–252 (2014).
- K. Daskalakis, S. Maier, R. Murray, S. Kéna-Cohen, Nonlinear interactions in an organic polariton condensate. *Nat. Mater.* **13**, 271–278 (2014).
- C. P. Dietrich, A. Steude, L. Tropic, M. Schubert, N. M. Kronenberg, K. Ostermann, S. Höfling, M. C. Gather, An exciton-polariton laser based on biologically produced fluorescent protein. *Sci. Adv.* **2**, e1600666 (2016).
- W. Xie, H. Dong, S. Zhang, L. Sun, W. Zhou, Y. Ling, J. Lu, X. Shen, Z. Chen, Room-temperature polariton parametric scattering driven by a one-dimensional polariton condensate. *Phys. Rev. Lett.* **108**, 166401 (2012).
- J. Fischer, I. G. Savenko, M. D. Fraser, S. Holzinger, S. Brodbeck, M. Kamp, I. A. Shelykh, C. Schneider, S. Höfling, Spatial coherence properties of one dimensional exciton-polariton condensates. *Phys. Rev. Lett.* **113**, 203902 (2014).
- B. Zhang, Z. Wang, S. Brodbeck, C. Schneider, M. Kamp, S. Höfling, H. Deng, Zero-dimensional polariton laser in a subwavelength grating-based vertical microcavity. *Light Sci. Appl.* **3**, e135 (2014).
- D. Bajoni, P. Senellart, E. Wertz, I. Sagnes, A. Miard, A. Lemaître, J. Bloch, Polariton laser using single micropillar GaAs-GaAlAs semiconductor cavities. *Phys. Rev. Lett.* **100**, 047401 (2008).
- T. Gao, P. S. Eldridge, T. C. H. Liew, S. I. Tsintzos, G. Stavriniadis, G. Deligeorgis, Z. Hatzopoulos, P. Savvidis, Polariton condensate transistor switch. *Phys. Rev. B* **85**, 235102 (2012).
- M. Klaas, H. Sigurdsson, T. C. H. Liew, S. Klembt, M. Amthor, F. Hartmann, L. Worschech, C. Schneider, S. Höfling, Electrical and optical switching in the bistable regime of an electrically injected polariton laser. *Phys. Rev. B* **96**, 041301 (2017).
- D. Ballarini, M. De Giorgi, E. Cancellieri, R. Houdré, E. Giacobino, R. Cingolani, A. Bramati, G. Gigli, D. Sanvitto, All-optical polariton transistor. *Nat. Commun.* **4**, 1778 (2013).
- H. S. Nguyen, D. Vishnevsky, C. Sturm, D. Tanese, D. Solnyshkov, E. Galopin, A. Lemaître, I. Sagnes, A. Amo, G. Malpuech, J. Bloch, Realization of a double-barrier resonant tunneling diode for cavity polaritons. *Phys. Rev. Lett.* **110**, 236601 (2013).
- T. Liew, A. V. Kavokin, I. A. Shelykh, Optical circuits based on polariton neurons in semiconductor microcavities. *Phys. Rev. Lett.* **101**, 016402 (2008).
- T. Espinosa-Ortega, T. C. H. Liew, Complete architecture of integrated photonic circuits based on AND and NOT logic gates of exciton polaritons in semiconductor microcavities. *Phys. Rev. B* **87**, 195305 (2013).
- E. Wertz, L. Ferrier, D. D. Solnyshkov, R. Johné, D. Sanvitto, A. Lemaître, I. Sagnes, R. Grousson, A. V. Kavokin, P. Senellart, G. Malpuech, J. Bloch, Spontaneous formation and optical manipulation of extended polariton condensates. *Nat. Phys.* **6**, 860–864 (2010).
- E. Wertz, A. Amo, D. D. Solnyshkov, L. Ferrier, T. C. H. Liew, D. Sanvitto, P. Senellart, I. Sagnes, A. Lemaître, A. V. Kavokin, G. Malpuech, J. Bloch, Propagation and amplification dynamics of 1D polariton condensates. *Phys. Rev. Lett.* **109**, 216404 (2012).
- T. Lecomte, V. Ardizzone, M. Abbarchi, C. Diederichs, A. Miard, A. Lemaître, I. Sagnes, P. Senellart, J. Bloch, C. Delalande, J. Tignon, P. Roussignol, Optical parametric oscillation in one-dimensional microcavities. *Phys. Rev. B* **87**, 155302 (2013).
- G. Dasbach, M. Schwab, M. Bayer, D. Krizhanovskii, A. Forchel, Tailoring the polariton dispersion by optical confinement: Access to a manifold of elastic polariton pair scattering channels. *Phys. Rev. B* **66**, 201201 (2002).
- Y. Sun, P. Wen, Y. Yoon, G. Liu, M. Steger, L. N. Pfeiffer, K. West, D. W. Snoke, K. A. Nelson, Bose-Einstein condensation of long-lifetime polaritons in thermal equilibrium. *Phys. Rev. Lett.* **118**, 016602 (2017).
- B. Nelsen, G. Liu, M. Steger, D. W. Snoke, R. Balili, K. West, L. Pfeiffer, Dissipationless flow and sharp threshold of a polariton condensate with long lifetime. *Phys. Rev. X* **3**, 041015 (2013).
- M. Steger, G. Liu, B. Nelsen, C. Gautham, D. W. Snoke, R. Balili, L. Pfeiffer, K. West, Long-range ballistic motion and coherent flow of long-lifetime polaritons. *Phys. Rev. B* **88**, 235314 (2013).
- M. Steger, C. Gautham, D. W. Snoke, L. Pfeiffer, K. West, Slow reflection and two-photon generation of microcavity exciton-polaritons. *Optica* **2**, 1–5 (2015).
- A. Gianfrate, L. Dominici, O. Voronich, M. Matuszewski, M. Stobińska, D. Ballarini, M. De Giorgi, G. Gigli, D. Sanvitto, Superluminal X-waves in a polariton quantum fluid. *Light Sci. Appl.* **7**, 17119 (2018).
- F. Manni, K. G. Lagoudakis, B. Pietka, L. Fontanesi, M. Wouters, V. Savona, R. André, B. Deveaud-Plédran, Polariton condensation in a one-dimensional disordered potential. *Phys. Rev. Lett.* **106**, 176401 (2011).
- G. Lerario, D. Ballarini, A. Fieramosca, A. Cannavale, A. Genco, F. Mangione, S. Gambino, L. Dominici, M. De Giorgi, G. Gigli, D. Sanvitto, High-speed flow of interacting organic polaritons. *Light Sci. Appl.* **6**, e16212 (2017).
- K. S. Daskalakis, S. A. Maier, S. Kéna-Cohen, Spatial coherence and stability in a disordered organic polariton condensate. *Phys. Rev. Lett.* **115**, 035301 (2015).
- G. Lerario, A. Fieramosca, F. Barachati, D. Ballarini, K. S. Daskalakis, L. Dominici, M. De Giorgi, S. A. Maier, G. Gigli, S. Kéna-Cohen, D. Sanvitto, Room-temperature superfluidity in a polariton condensate. *Nat. Phys.* **13**, 837–841 (2017).
- R. Su, C. Diederichs, J. Wang, T. C. H. Liew, J. Zhao, S. Liu, W. Xu, Z. Chen, Q. H. Xiong, Room-temperature polariton lasing in all-inorganic perovskite nanoplatelets. *Nano Lett.* **17**, 3982–3988 (2017).
- Q. Zhang, R. Su, X. Liu, J. Xing, T. C. Sum, Q. H. Xiong, High-quality whispering-gallery-mode lasing from cesium lead halide perovskite nanoplatelets. *Adv. Funct. Mater.* **26**, 6238–6245 (2016).
- S. T. Ha, X. Liu, Q. Zhang, D. Giovanni, T. C. Sum, Q. H. Xiong, Synthesis of organic-inorganic lead halide perovskite nanoplatelets: Towards high-performance perovskite solar cells and optoelectronic devices. *Adv. Opt. Mater.* **2**, 838–844 (2014).
- S. Zhang, Q. Shang, W. Du, J. Shi, Z. Wu, Y. Mi, J. Chen, F. Liu, Y. Li, M. Liu, Strong exciton-photon coupling in hybrid inorganic-organic perovskite micro/nanowires. *Adv. Opt. Mater.* **6**, 1701032 (2018).
- T. J. S. Evans, A. Schlaus, Y. Fu, X. Zhong, T. L. Atallah, M. S. Spencer, L. E. Brus, S. Jin, X.-Y. Zhu, Continuous-wave lasing in cesium lead bromide perovskite nanowires. *Adv. Opt. Mater.* **6**, 1700982 (2018).
- E. Kammann, T. C. H. Liew, H. Ohadi, P. Cilibizzi, P. Tsotsis, Z. Hatzopoulos, P. G. Savvidis, A. V. Kavokin, P. G. Lagoudakis, Nonlinear optical spin Hall effect and long-range spin transport in polariton lasers. *Phys. Rev. Lett.* **109**, 036404 (2012).

Acknowledgments

Funding: Q.X. acknowledges the support from the Singapore National Research Foundation through the NRF Investigatorship Award (NRF-NRFI2015-03) and the Singapore Ministry of Education via AcRF Tier 2 grant (MOE2015-T2-1-047) and Tier 1 grants (RG103/15 and RG113/16). T.C.H.L. acknowledges the support of the Singapore Ministry of Education via AcRF Tier 2 grant (MOE2017-T2-1-001). **Author contributions:** Q.X. supervised the research. R.S. conceived the idea, designed the research, and performed the DBR fabrication, sample growth, and all the optical measurements. J.Z. and J.X. carried out the atomic force microscopy measurements. T.C.H.L. carried out all the theoretical calculations. R.S., J.W., C.D., T.C.H.L., and Q.X. analyzed the data. R.S., T.C.H.L., and Q.X. wrote the manuscript. All authors commented on the manuscript. **Competing interests:** The authors declare that they have no competing interests. **Data and materials availability:** All data needed to evaluate the conclusions in the paper are present in the paper and/or the Supplementary Materials. Additional data related to this paper may be requested from the authors. Correspondence and requests for materials should be addressed to the authors.

Submitted 29 April 2018

Accepted 18 September 2018

Published 26 October 2018

10.1126/sciadv.aau0244

Citation: R. Su, J. Wang, J. Zhao, J. Xing, W. Zhao, C. Diederichs, T. C. H. Liew, Q. Xiong, Room temperature long-range coherent exciton polariton condensate flow in lead halide perovskites. *Sci. Adv.* **4**, eaau0244 (2018).

Room temperature long-range coherent exciton polariton condensate flow in lead halide perovskites

Rui Su, Jun Wang, Jiaxin Zhao, Jun Xing, Weijie Zhao, Carole Diederichs, Timothy C. H. Liew and Qihua Xiong

Sci Adv 4 (10), eaau0244.
DOI: 10.1126/sciadv.aau0244

ARTICLE TOOLS <http://advances.sciencemag.org/content/4/10/eaau0244>

SUPPLEMENTARY MATERIALS <http://advances.sciencemag.org/content/suppl/2018/10/22/4.10.eaau0244.DC1>

REFERENCES This article cites 41 articles, 2 of which you can access for free
<http://advances.sciencemag.org/content/4/10/eaau0244#BIBL>

PERMISSIONS <http://www.sciencemag.org/help/reprints-and-permissions>

Use of this article is subject to the [Terms of Service](#)

Science Advances (ISSN 2375-2548) is published by the American Association for the Advancement of Science, 1200 New York Avenue NW, Washington, DC 20005. 2017 © The Authors, some rights reserved; exclusive licensee American Association for the Advancement of Science. No claim to original U.S. Government Works. The title *Science Advances* is a registered trademark of AAAS.